Published in final edited form as:
J Immunol. 2013 April 1; 190(7): 3447–3457. doi:10.4049/jimmunol.1200604.

Implicating Exudate Macrophages and Ly-6C^{high} Monocytes in CCR2-Dependent Lung Fibrosis Following Gene-Targeted Alveolar Injury[1]

John J Osterholzer[*,†,‡,§,2], **Michal A Olszewski**[†,‡,§], **Benjamin J Murdock**[§], **Gwo-Hsiao Chen**[§], **John Erb-Downward**[§], **Natalya Subbotina**[§], **Keely Browning**[§], **Yujing Lin**[§], **Roger E. Morey**[†], **Jeremy K. Dayrit**[†], **Jeffrey C. Horowitz**[§], **Richard H. Simon**[§], and **Thomas H. Sisson**[§]

[*]Pulmonary Section, Medical Service, University of Michigan Health System, Ann Arbor, MI

[†]Research Service, Ann Arbor VA Health System, Department of Veterans Affairs Health System, University of Michigan Health System, Ann Arbor, MI

[‡]Graduate Program in Immunology, University of Michigan Health System, Ann Arbor, MI

[§]Division of Pulmonary & Critical Care Medicine, Department of Internal Medicine, University of Michigan Health System, Ann Arbor, MI

Abstract

The alveolar epithelium is characteristically abnormal in fibrotic lung disease, and we recently established a direct link between injury to the type II alveolar epithelial cell (AEC) and the accumulation of interstitial collagen. The mechanisms by which damage to the epithelium induces lung scarring remain poorly understood. It is particularly controversial whether an insult to the type II AEC initiates an inflammatory response that is required for the development of fibrosis. To explore whether local inflammation occurs following a targeted epithelial insult and contributes to lung fibrosis, we administered diphtheria toxin to transgenic mice with type II AEC-restricted expression of the diphtheria toxin receptor. We employed immunophenotyping techniques and diphtheria toxin receptor-expressing, chemokine-receptor-2 deficient (CCR2−/−) mice to determine the participation of lung leukocyte subsets in pulmonary fibrogenesis. Our results demonstrate that targeted type II AEC injury induces an inflammatory response that is enriched for CD11b+ non-resident exudate macrophages (ExM) and their precursors, Ly-6C^{high} monocytes. CCR2-deficiency abrogates the accumulation of both cell populations and protects mice from fibrosis, weight loss, and death. Further analyses revealed that the ExM are alternatively-activated and that ExM and Ly-6C^{high} monocytes express mRNA for IL-13, TGF-β, and the collagen genes, COL1A1 and COLIIIA1. Furthermore, the accumulated ExM and Ly-6C^{high} monocytes contain intracellular collagen as detected by immunostaining. Together, these results implicate CCR2 and the accumulation of ExM and Ly-6C^{high} monocytes as critical determinants of pulmonary fibrosis induced by selective type II AEC injury.

Address all Correspondence to: John J. Osterholzer, M.D., Pulmonary and Critical Care Medicine Section (111G), Department of Veterans Affairs Medical Center, 2215 Fuller Road, Ann Arbor, MI 48105-2303 U.S.A, Phone: 734-845-5080, FAX: 734-845-3257, oster@umich.edu.

[1]Supported by a Career Development Award-2 (J.J.O) from the Biomedical Laboratory Research & Development Service, Department of Veterans Affairs and by National Institutes of Health Grants R01 HL078871 (THS) and R01HL105489 (JCH), and the Quest For Breath Foundation (THS).

[2]Address correspondence and reprint requests to: John J. Osterholzer. M.D., Pulmonary and Critical Care Medicine Section (111G), Department of Veterans Affairs Hospital, 2215 Fuller Road, Ann Arbor, MI 48105-2303. oster@umich.edu.

[3]Portions of this manuscript were presented at the International Conference of the American Thoracic Society, May, 2011, Denver CO and published in abstract form: Am J Respir Crit Care Med 183;2011:A6148

Keywords

Pulmonary; Collagen; Inflammation; CCR2; Alveolar Epithelium

Introduction

Idiopathic Pulmonary Fibrosis (IPF) is a chronic progressive scarring disorder of the lung. Treatment options for IPF and other fibrotic lung diseases are limited and the identification of new therapeutic targets would be aided by an improved understanding of disease pathogenesis. Numerous indirect observations suggest that abnormalities of the alveolar epithelium, and in particular type II alveolar epithelial cells (AECs), precipitate the fibrotic cascade. For example, epithelial cell hyperplasia and denudation are commonly observed overlying the fibroblast foci, the purported sites of active collagen deposition in the IPF lung (1–3). In addition, mutations in type II AEC-specific genes including surfactant protein A2, surfactant protein C (SPC), and ATP-binding cassette protein A3 have been linked to familial fibrotic lung disease (4–8). Similar to the human disease, defects in the alveolar epithelium are prominent in the murine model of bleomycin-induced pulmonary fibrosis (9, 10). To substantiate the direct link between defects in the alveolar epithelium and fibrogenesis, we developed transgenic mice that express the human diphtheria toxin receptor (DTR) in a type II AEC specific manner. We found that the administration of diphtheria toxin (DT) to these mice selectively injured their type II AECs and induced pulmonary fibrosis (11).

The mechanism(s) by which AEC injury instigates pulmonary fibrosis remains uncertain. Although early studies implicated lung inflammation in the pathogenesis of IPF, a current prevailing hypothesis proposes that repetitive damage to the alveolar epithelium, with little contribution from inflammatory cells, results in collagen accumulation by preventing normal wound repair and by stimulating the secretion of profibrotic growth factors (12). However, recent reports have spurred a renewed scientific interest in the role of inflammation, and specifically macrophages, in the development of fibrotic lung disease. For example, macrophage accumulation can be a prominent feature in individuals with familial pulmonary fibrosis due to SPC and ATP-binding cassette protein A3 mutations (6, 8). In addition, macrophage accumulation has been observed in several murine models of lung fibrosis (e.g. bleomycin administration, γ-herpes virus infection, transforming growth factor-β (TGF-β) overexpression, and interleukin-10 overexpression) (13–19). Despite the recognition that macrophages are present in areas of injury in these models, little is known about their phenotype or whether they are derived from local or circulating precursors. Our recent study was the first to directly show that targeted alveolar injury was necessary and sufficient to induce non-resident exudate macrophage accumulation in mice that develop lung fibrosis (20). In this study, we implicated macrophage gene expression of PAI-1 and Collagen-1 as potential mechanisms by which these cells promote lung scarring. Despite these advances, many questions still remain including the mechanism by which the ExM accrue within the lung microenvironment and how they promote fibrogenesis.

In the current study, we undertook a detailed kinetic analysis of macrophage and monocyte accumulation in mice in response to targeted type II AEC injury. Our results demonstrate that fibrosis following alveolar damage occurs in conjunction with the increased accrual of non-resident exudate macrophages (ExM) and their precursors, Ly-6C^{high} monocytes. A thorough phenotypic analysis reveals that the ExM and Ly-6C^{high} monocyte subpopulations demonstrate a profibrotic phenotype characterized by alternative activation and the expression of both profibrotic cytokines and collagen. Furthermore, CCR2-deficiency limits the macrophage/monocyte accumulation and protects against collagen deposition.

Collectively, our results provide important insights into how epithelial injury is translated into interstitial fibrosis, and we elucidate specific cell types and cell recruitment pathways that might serve as novel therapeutic targets for patients with IPF.

Methods

Animals

All animal experiments were performed in accordance with institutional guidelines set forth by the University Committee on the Use and Care of Animals. Transgenic mice expressing the diphtheria toxin receptor (DTR) under the control of the murine SPC promoter were generated in our laboratory on a C57BL/6 background (designated DTR+ mice) (11). Control C57BL/6 mice (WT) were purchased from Jackson Laboratories (Bar Harbor, ME). We sequentially crossed DTR+ mice with $CCR2^{-/-}$ mice (C57BL/6 genetic background) to generate CCR2-deficient DTR+ (DTR+/$CCR2^{-/-}$) mice.

Assessment of mouse genotypes

The presence of the DTR was detected using PCR as previously described (11).

Diphtheria Toxin Administration and Experimental Design

Six to eight week old mice (from the strains identified above) were intraperitoneally injected with DT (Sigma Chemical, St. Louis, MO) once daily for 14 days at a dose of 10.0 μg/kg in 100 μl of PBS (or PBS alone). Note that DT administration selectively injures type II alveolar epithelial cells in transgenic mice expressing the diphtheria toxin receptor off the promoter for surfactant protein C (DTR+ mice (11, 20). At timepoints designated in specific studies, mice were assessed for one or more of the following experimental parameters: 1) Total lung leukocyte and lung leukocyte subset accumulation (by flow cytometric analysis and histology; 2) Whole lung gene expression (by multiplex quantitative PCR array); 3) Lung collagen content and microanatomic location (by hydroxyproline content and immunohistochemistry); 4) Weight loss; 5) Survival; and 6) Lung macrophage and monocyte phenotype (by flow cytometric analysis and specific mRNA expression by quantitative RT-PCR performed on specific cell subsets purified by fluorescence- activated cell sorting).

Tissue Collection

Lungs were perfused via the right heart using 5 ml of PBS containing 0.5 mM EDTA. Lungs were then excised, minced, and enzymatically digested to obtain a single cell suspension of lung leukocytes as previously described (21).

Multiplex quantitative PCR Array

RNA was purified from lung leukocytes by the TRIzol method (Ambion), and cDNA was generated using the RT^2 First Strand Kit (Qiagen). 2.5 ng of cDNA from each sample were loaded into the wells of a custom QPCR array (Quiagen) and run on a LightCycler 480 system (Roche). Relative RNA expression levels were inferred from the C_t values using β-actin as the control. Significant genes were identified using R-package samr which utilizes the false-discovery rate method employed in the software SAM (Significance Analysis of Microarrays) (22).

Monoclonal antibodies

The following mAbs were purchased from BioLegend (San Diego, CA): N418 (anti-murine CD11c, hamster IgG1); 2.4G2 (“Fc block”) (anti-murine CD16/CD32, rat IgG2b); 30-F11 (anti-murine CD45, rat IgG2b); 16–10A1 (anti-murine CD80, hamster IgG2); GL1 (anti-

murine CD86, rat IgG2a); MIH5 (anti-murine B7-H1/PDL-1, rat IgG2a); TY25 (anti-murine B7-DC/PDL-2, rat IgG2a); AMS-32.1 (anti- murine I-A^d "MHC Class II", mouse IgG2b); 145–2C11 (anti-murine CD3ε, hamster IgG1, κ); 6D5 (anti-murine CD19, rat IgG2a); M3/38 (anti-murine Mac-2, rat IgG2a); M3/84 (anti-murine CD107b (Mac-3), rat IgG1); 1A8 (anti-Ly-6G, rat IgG2a) BM8 (anti-murine F4/80, rat IgG2a) and TG12 (anti-murine CXCR4, rat IgG2b). The following mAbs were purchased from BD Biosciences PharMingen (San Diego, CA): AL-21 (anti-murine Ly-6C, Rat IgM); M1/70 (anti-murine CD11b, rat IgG2b), and 3/23 (anti-murine CD40, rat IgG2a). The following mAbs were purchased from Cedarlane Laboratories (Burlington, NC): 2F8 (anti-murine CD204, rat IgG2b), and NLDC-145 (anti-Murine CD205, rat IgG2a). The following mAb were purchased from Rockland Immunochemicals (Gilbertsville, PA): anti-collagen (#600-401-103) and Jackson Immunoresearch: Rabbit IgG (#011-000-003) and Donkey anti-rabbit Ig (-#711-166-152). The mAbs were primarily conjugated with FITC, PE, PerCP-Cy5.5, allophycocyanin, allophycocyanin-Cy7, or Pacific Blue. Isotype-matched irrelevant control mAbs (BioLegend) were tested simultaneously in all experiments.

Antibody staining and flow cytometric analysis

Antibody staining, including blockade of Fc receptors, and analysis by flow cytometry were performed as described previously (20, 23, 24). Data was collected on a BD LSR II flow cytometer equipped with 488-nm blue, 405-nm violet, and 633-nm red lasers using FACSDiva software (both from Becton Dickinson Immunocytometry Systems, Mountain View, CA) and analyzed using FlowJo software (Tree Star Inc., San Carlos, CA). 10,000 to 100,000 cells were analyzed per sample. In selected experiments, fluorescence activated cell sorting of specific lung macrophage populations was performed using a BD ARIA flow cytometer and FACSDiva software.

Gating strategy used to identify lung leukocyte subsets including macrophages and monocytes

Single cell suspensions enriched for lung leukocytes were obtained, antibody-stained, and assessed by flow cytometry (as above) using a previously published gating strategy (20, 24, 25) detailed in Supplemental Figure S1. To identify lung macrophages and monocytes (Figure S1A), samples were stained with anti-Ly-6C (FITC), anti-F4/80 (PE), anti-CD3 and anti-CD19 (PerCP Cy5.5), anti-Ly-6G (PE-allophycocyanin-Cy7), anti-CD45 (allophycocyanin), anti-CD11b (allophycocyanin-Cy7), and anti-CD11c (Pacific Blue). Thereafter, a series of gates were used to identify alveolar macrophages (AM; $CD45^+$ $CD3^-$ $CD19^-$ Ly-$6G^-$ $FSC^{mod/high}$ $autofluorescent^+$ $CD11c^+$ $CD11b^-$), exudate macrophages (ExM; $CD45^+$ $CD3^-$ $CD19^-$ Ly-$6G^-$ $FSC^{mod/high}$ $autofluorescent^+$ $CD11c^+$ $CD11b^+$), Ly-$6C^{high}$ monocytes ($CD45^+$ $CD3^-$ $CD19^-$ SSC^{low} $CD11c^-$ $F4/80^+$ $CD11b^+$ Ly-$6C^{high}$), and Ly-$6C^{low}$ monocytes ($CD45^+$ $CD3^-$ $CD19^-$ SSC^{low} $CD11c^-$ $F4/80^+$ $CD11b^+$ Ly-$6C^{low}$). In some experiments, further antibody staining was performed to evaluate these leukocyte subsets for cell surface markers commonly expressed on macrophages and monocytes (refer to Figure 5A–B and 6E). To identify granulocytes (Figure S1B), a series of gates were set to identify neutrophils ($CD45^+$ $SSC^{mod/high}$ Ly-$6G^{high}$) and eosinophils ($CD45^+$ $FSC^{low/mod}$ SSC^{high}, Ly-$6G^{mod}$). To identify lymphocytes (Figure S1C), separate samples were stained with anti-CD8 (FITC), anti-CD4 (PE), anti-CD19 (PerCP Cy5.5) and anti-CD45 (allophycocyanin) to identify CD4+ T cells (CD45+ CD4+), CD8+ T cells (CD45+ CD8+) and B cells (CD45+ CD19+).

Monocyte/Macrophage isolation

Myeloid cell subsets from DTR+ mice (n=5) following 14 days of DT treatment were purified (≈95%) by fluorescence-activated cell sorting using the gating strategy described above (Figure S1A and (20, 24).

Quantitative RT-PCR on sorted macrophages and monocytes

Total macrophage or monocyte-specific RNA was prepared using RNeasy Plus Mini Kit (Qiagen) and first-strand cDNA was synthesized using SuperScriptIII (Invitrogen, Carlsbad, CA). Specific qPCRs were conducted using a SYBR Green-based detection and a MX 3000P system (Stratagene, La Jolla, CA). Forty cycles were performed (94°C for 15 seconds followed by 60°C for 30 seconds and 72°C for 30 seconds) using each cDNA template. The mRNA levels were normalized with the expression of the housekeeping GAPDH using the following formula: %GAPDH expression = $100/2^{-\Delta\Delta C_T}$. Data is presented as an average ± SEM of 3 individual experiments (with each experiment representing gene expression on leukocyte subsets pooled from 5 DT-treated DTR+ mice). The following primer pairs were used for qRT-PCR detection of mRNA expression: Arg-1 sense, CAGAAGAATGGAAGAGTCAG; Arg-1 antisense, CAGATATGCAGGGAGTCACC; Galectin-3 sense, TCTTCATCCGATGGTTGTACTG, Galectin-3 antisense, TTTCAGGAGAGGGAATGATGTT; inducible NO synthase (iNOS) sense, TTTGCTT-CCATGCTAATGCGAAAG; iNOS antisense, GCTCTGTTGAGGTCTAAAGGCTCCG; IL-13 sense, CTACAGCTCCCTGGTTCTCT, IL-13 antisense, TTGCTCAGCTCCTCA-ATAAG; TGF-β, TGTACGGCAGTGGCTGAACCAA, TGF-β antisense, CGCTGAATC-GAAAGCCCTGTATT; COL1a1 sense, ACCTCAAGATGTGCCACTCTGACTG, COL1a1 antisense, GCAGCCTTGGTTAGGGTCGATC, COL3a1 sense, CAATCCAGGTCCTCC-AGGTTCTC, COL3a1 antisense, ACCTGCAGGTCCTGGACTACCAA; GAPDH sense, TATGTCGTGGAGTCTACTG; GAPDH antisense, GAGTTGTCATATTTCTCGT.

Hydroxyproline assay

Hydroxyproline content of the lung was measured as previously described (26).

Lung histology

The left lung was inflation-fixed at 25 cm H_2O pressure with 10% neutral-buffered formalin, removed *en bloc*, further fixed in 10% neutral-buffered formalin overnight, and then paraffin embedded. Five micron sections were stained using haemotoxylin and eosin or picrosirius red and visualized by bright field and cross-polarized microscopy.

Statistical Analysis

All data were expressed as mean ± SEM. Data were evaluated by unpaired Student's t-test (for comparison between two samples) or by ANOVA with Dunnett's post test (for multiple comparisons). Statistical difference was accepted at $p<0.05$.

Results

Targeted type II alveolar epithelial cell injury induces lung inflammation

In this murine model, repetitive administration (for 14 days) of diphtheria toxin (DT) to transgenic mice expressing the diphtheria toxin receptor (DTR) off of the surfactant protein C promoter (DTR+ mice) selectively injures type II alveolar epithelial cells (AEC) and results in pulmonary fibrosis as evidenced by increased lung hydroxyproline content and histologic evidence of collagen deposition in alveolar regions (11). Although we have found PAI-1 to be required, the mechanisms translating AEC injury into lung fibrosis in this model have not been determined. In the present study, we first investigated whether a targeted type II AEC injury would induce inflammation. Using flow cytometric analysis, we enumerated the total number of CD45+ leukocytes within the lungs of both WT and DTR+ mice before (day 0), during (day 7 and day 14), and one week after (day 21) DT treatment. Total lung

leukocytes did not increase in WT mice treated with DT whereas, in DTR+ mice, the number of CD45+ cells were significantly increased (~2 fold; Figure 1A).

We next compared histologic features of injury on day 14 in DT-treated WT and DTR+ mice. As expected, no evidence of alveolar damage or inflammation was evident in the WT group (Figure 1B; left panel). In contrast, patchy areas of interstitial thickening were prevalent in the lungs of DT-treated DTR+ mice, and these regions contained numerous large cells with macrophage morphology (Figure 1B; right panel and inset).

Lastly, we performed a limited gene array on the total lung leukocyte population obtained from DT-treated WT and DTR+ mice (at D14) to further characterize this inflammatory response. Of the 20 genes assessed, we found an up-regulation of Arginase-1 and a decreased expression of interferon-gamma in DTR+ mice (relative to WT mice) (Figure 1C).

Exudate macrophages and Ly-6C^{high} monocyte accumulation

The identification of large cells within the injured alveoli and the increase in Arginase-1 expression in DT-treated DTR+ mice suggested to us that macrophages might be accumulating in response to the targeted type II AEC injury. To evaluate this possibility, we used flow cytometric analysis with an established gating strategy ((20, 24) and as described in Methods and Figure S1; abbreviated gating shown in Figure 2A–C) to distinguish and enumerate alveolar macrophages (AM) and exudate macrophages (ExM) in the lungs of DT-treated WT and DTR+ mice. Prior studies indicate that AM are predominantly resident cells while ExM accumulate in the lung in response to infection and inflammation (24, 27–29). Consistent with this, we found a modest increase in the AM population (~1–2 fold) in DTR+ mice at day 7 of DT treatment (relative to untreated DTR+ mice) that did not differ from DT-treated WT mice at any time point (Figure 2D). In contrast, the number of ExM: a) increased nearly 5-fold (relative to untreated DTR+ mice), b) peaked on day 14 of DT treatment, and c) differed significantly from DT-treated WT mice on day 14 and 21 of treatment (Figure 2E). Note that DT treatment induced a small (~2 fold) and transient (D7 only) increase in AM and ExM numbers in WT mice. The observed expansion of ExM in the DT-treated DTR+ mice was unique as other lung leukocyte subsets were either not increased (CD4$^+$ T cells and eosinophils) or increased less than 2-fold (CD8$^+$ T cells, B cells, and neutrophils) (relative to DT-treated WT mice; Figure S2).

We hypothesized that the observed increase in ExM population in response to alveolar injury was due to the recruitment of an ExM precursor. We and others previously demonstrated that ExM are derived from Ly-6C^{high} monocytes (24, 28, 30). However, both Ly-6C^{high} monocytes (which are CCR2+ CX3CR- and often referred to as “inflammatory monocytes”) and Ly-6C^{low} monocytes (which are CCR2- CX3CR+ and often referred to as “patrolling monocytes”) have been identified at sites of tissue fibrosis in murine models (15, 27). Using flow cytometric analysis (as described in Methods and Figure S1; abbreviated gating shown in Figure 2F–H), we identified both Ly-6C^{high} and Ly-6C^{low} monocytes in the lungs of DT-treated DTR+ mice (Figure 2F–H). The Ly-6C^{high} monocytes increased >4-fold in DT-treated DTR+ mice after 7 days (relative to untreated DTR+ mice; Figure 2I) immediately preceding the peak accumulation of ExM (refer to Figure 2E). In comparison, there was no increase in this leukocyte population in DT treated WT mice. In contrast, Ly-6C^{low} monocytes were not increased at D7 in DT-treated DTR+ mice and only increased 2-fold by D14 of treatment (Figure 2J). Collectively, these data demonstrate that a selective injury to the type II alveolar epithelium is sufficient to promote the accrual of Ly-6C^{high} monocytes and implies that these cells locally differentiate into ExM following their recruitment.

The role of CCR2 in exudate macrophages and Ly-6C^{high} accumulation

Prior studies indicate that the lung accumulation of ExM and Ly-6C^{high} monocytes in response to infectious stimuli is CCR2-dependent (24, 25, 28, 29). To assess the role of CCR2 in our alveolar injury model, we evaluated macrophage and monocyte accumulation following DT treatment in CCR2-deficient DTR+ (DTR+:CCR2−/−) mice. Our results demonstrate the expected increase in ExM (Figure 3A) and Ly-6C^{high} monocytes (Figure 3B) in the DTR+:CCR2-expressing mice relative to control animals (at D14). In contrast, the numbers of ExM and Ly-6C^{high} monocytes did not increase in CCR2-deficient DTR+ mice (Figure 3A, 3B). Consistent with these cell counts, we observed with light microscopy no evidence of increased interstitial macrophage accumulation in the lungs of DT-treated CCR2-deficient DTR+ mice on day 14 (Figure 3C; refer to Figure 1B for comparisons with similarly-treated WT and DTR+ mice). Note that CCR2 deficiency did not influence the numbers of AM or Ly-6C^{low} monocytes (*data not shown*).

The role of CCR2 in targeted type II AEC injury-induced lung fibrosis, weight loss, and mortality

We next assessed the influence of CCR2 on lung fibrosis following targeted type II AEC injury. We compared lung hydroxyproline content in the following four groups of DT-treated mice: 1) WT (DTR−:CCR2+/+), 2) CCR2-deficient (DTR−:CCR2−/−), 3) DTR+ (DTR+:CCR2+/+), and 4) CCR2-deficient DTR+ (DTR+:CCR2−/−). A control group of PBS-treated WT mice was included to establish basal lung collagen content. As was the case in our original study, DT treatment of WT mice did not significantly increase lung hydroxyproline content (CI of −64.09 to +8.724 mcg/ml, Figure 4A)(11). CCR2-deficient mice (that were negative for DTR) also did not develop a significant increase in lung collagen content with DT exposure. In contrast, DT treatment of DTR+ mice with intact CCR2 expression induced a robust (>2-fold) increase in lung hydroxyproline consistent with our prior studies (11, 20). Importantly, this increase in the quantity of lung hydroxyproline in the DT-treated DTR+ mice was abrogated by the absence of CCR2 expression, and the lung hydroxyproline content of these DT-treated DTR+:CCR2−/− mice was not different from the DT-treated control groups.

The quantitative changes in lung collagen content we observed were associated with qualitative changes in alveolar histology. Specifically, the lungs of DT-treated DTR+ mice demonstrated mixed cellular and fibrotic regions characterized by thickened alveolar walls and evidenced of increased alveolar wall collagen as assessed by picrosirius staining using bright field microscopy (Figure 4B, middle panels). Histologic evidence of increased lung collagen was not observed in DT-treated WT (Figure 4B, left panel) or CCR2-deficient DTR + mice (Figure 4B, right panels). Review of lung sections obtained from DTR+ mice under cross-polarized light (in which cross-aligned collagen is birefringent) provided additional evidence that the observed picrosirius staining was attributable to collagen (Figure 4C). The intensity of this staining was generally less than that observed surrounding larger airways and vascular structures suggesting that the newly deposited collagen may be loosely organized. Collectively, these results show that fibrosis resulting from a targeted epithelial injury is CCR2-dependent.

We previously demonstrated that mice with targeted type II AEC injury experienced significant weight loss and decreased survival (11, 20). To determine the effect of CCR2-deficiency on these parameters, weight loss and survival were monitored in the following 3 groups of mice treated with DT for 14 days: 1) WT mice (DTR−:CCR2+/+), 2) DTR+ mice (DTR+:CCR2+/+), and 3) CCR2-deficient DTR+ mice (DTR+:CCR2−/−). As expected, DT treatment to DTR+ mice resulted in weight loss (Figure 4C) and increased mortality (Figure 4D) relative to WT mice. In contrast, DT-treated CCR2-deficient DTR+ mice lost an

intermediate amount of weight (relative to DTR+ and WT mice) and were protected against the lethal effects of DT-mediated type II AEC injury.

Cell surface phenotype of the accumulated exudate macrophages and Ly-6C^{high} monocytes

Our results revealed a strong association between the accumulation of ExM and Ly-6C^{high} monocytes and the development of lung fibrosis following targeted alveolar injury. To gain additional insight into the phenotype and function of these cell populations, we next characterized their cell surface expression of: a) a panel of macrophage associated proteins (F4/80, Mac-2, Mac-3, CD204, CD205; Figure 5A); and b) MHC class II and co-stimulatory molecules (including CD40, CD80, CD86, and Programmed Cell Death Ligands 1 and 2; Figure 5B). Relative to their Ly-6C^{high} monocyte precursors, ExM expressed higher amounts of Mac-2, Mac-3, and CD204. Both populations expressed F4/80 but minimal CD205 (Figure 5A). ExM also expressed higher amounts of MHC Class II and costimulatory molecules than Ly-6C^{high} monocytes (Figure 5B).

Exudate macrophages are alternatively-activated and express mRNA for profibrotic cytokines

In macrophages, increased arginase expression relative to inducible nitric oxide synthase (iNOS) is characteristic of alternative activation, and this phenotype has been associated with tissue repair and fibrosis (15–17, 19, 31). We identified that Arginase-1 gene expression was up-regulated in the total lung leukocyte population obtained from DT-treated DTR mice (relative to DT-treated WT mice; Figure 1C). To determine whether this reflected alternative macrophage activation, we isolated (by cell sorting) pooled populations of ExM from DT-treated DTR+ mice (at D14) and used qRT-PCR to assess mRNA expression of Arginase-1 and Galectin-3 (associated with alternative activation) and iNOS (associated with classical activation). Results show that expression of Arginase, Galectin-3 (Figure 5C) and the Arginase:iNOS ratio (Figure 5D) were high in ExM (Figure 5C) obtained from DTR + mice consistent with an alternatively-activated phenotype. We also examined the expression of pro-fibrotic mediators by the ExM and Ly-6C^{high} monocytes and found that these cell populations expressed mRNA for interleukin-13 (IL-13) and TGF-β (Figure 5E). Collectively, our finding that ExM in the lungs of mice with targeted alveolar injury are alternatively-activated and express profibrotic cytokines suggests potential mechanisms by which these cells might contribute to pulmonary fibrosis.

Exudate macrophages and Ly-6C^{high} monocytes display evidence of collagen production

We next sought to determine whether lung leukocytes might directly influence the severity of fibrosis through collagen production. Detection of intracellular type I collagen staining by flow cytometric analysis has been used as evidence that CD45+ leukocytes express collagen (32–35). We therefore used antibody staining for intracellular Collagen-1 (Col1) and flow cytometric analysis to compare the percentage and total number of Col1+ cells amongst either CD45+ cells (leukocytes) or CD45- cells (non-leukocytes) obtained from the lungs of DT-treated: 1) WT mice, 2) DTR+ mice, or 3) DTR+:CCR2−/−mice (D14 of DT treatment). The percent of CD45+ cells staining positive for intracellular Col1 was similar between groups (WT mice = 4.4±0.4%; DTR+ mice = 4.7±0.2%; DTR+:CCR2−/− mice = 5.1±0.4%). However, the total number of Col1+ CD45+ cells (lung leukocytes) was significantly increased in DT-treated DTR+ mice but not DTR+:CCR2−/− mice (relative to WT mice; Figure 6A). The percent of CD45- cells staining for intracellular Col1 also did not significantly differ between groups (WT mice = 19.9±0.8%; DTR+ mice = 22.7±1.6%; DTR +:CCR2−/− mice = 19.9±1.4%) nor were there differences in the total number of Col1+ CD45- cells (non-leukocytes) between groups of mice (Figure 6A).

Next, we performed a similar analysis using our established gating strategy (Refer to Figures 2 and S1) to assess for intracellular Collagen-1 staining on subsets of lung macrophages and monocytes. We observed that ExM consistently display the highest percentage of type I collagen positive (Col1+) staining (24.5 ± 2.5%) in DTR+ mice in comparison to AM (13.1 ± 1.4%), Ly-6C^{high} monocytes (15.0 ± 1.4%), or Ly-6C^{low} monocytes (8.3 ± 1.9%) (Figure 6B). The percent of each subset staining positive for intracellular Col1 was similar between groups of mice (data not shown). However, the total numbers of Col1+ AM, ExM, and Ly-6C^{high} monocytes (but not Ly-6C^{low} monocytes) increased in DT-treated DTR+ mice (relative to WT mice) (Figure 6C). In contrast, the numbers of Col1+ ExM and Ly-6C^{high} monocytes in the lungs of CCR2-deficient DTR+ mice (which are protected from fibrosis) were significantly lower and similar to that of the WT group.

To determine whether intracellular collagen staining might be explained solely by collagen ingestion, we measured type I and type III collagen gene expression (by qRT-PCR) in these populations following their isolation (by fluorescence-activated cell-sorting) from DTR+ mice following 14 days of DT treatment. Results demonstrate strong expression of COL1A1 and COL3A1 genes in all four macrophage and monocyte subsets (Figure 6D) consistent with our findings using flow cytometric analysis.

Fibrocytes are bone marrow derived cells implicated in tissue fibrosis. They are broadly defined as cells staining for both the leukocyte cell surface marker CD45 and intracellular collagen and their accumulation in the lungs of mice subjected to bleomycin injury is CCR2-dependent (23, 36, 37). Thus, the Col1+ ExM and Ly-6C^{high} monocytes we observed in the lungs of DT-treated DTR+ mice qualify as fibrocytes by these criteria. To determine if these cells expressed another fibrocyte marker, we assessed for C-X-C chemokine receptor type 4 (CXCR4) mRNA (36). Our results demonstrate that ExM and Ly-6C^{high} monocytes obtained from DT-treated DTR+ mice express low to modest amounts of CXCR4 (Figure 6E).

Discussion

In the present study, we used transgenic mice expressing the diphtheria toxin (DT) receptor under the control of the surfactant protein C promoter to investigate whether DT-mediated injury of the alveolar epithelium would result in lung inflammation, and if so, what specific inflammatory cells subsets participate in the development of lung fibrosis in this model system. We report the following novel findings: 1) Repetitive DT-mediated injury to type II alveolar epithelial cells results in an inflammatory response enriched for non-resident ExM and Ly-6C^{high} monocytes; 2) ExM and Ly-6C^{high} monocytes do not accumulate in the lungs of DTR+:CCR2−/− transgenics, and these mice are protected from lung fibrosis, weight loss, and death in response to DT-treatment; 3) ExM and Ly-6C^{high} monocytes demonstrate alternative activation and profibrotic cytokine production, potential mechanisms whereby these cells might promote fibrogenesis; and 4) ExM and Ly-6C^{high} monocytes meet criteria for fibrocytes.

The pathogenic underpinnings of pulmonary fibrosis remain poorly understood. Consistently recognized abnormalities of the alveolar epithelium in areas of ongoing fibrosis have served as the basis for the popular hypothesis that pulmonary fibrosis results from aberrant wound repair (12). In this hypothesis, the contribution of inflammation to lung scarring is downplayed in part because anti-inflammatory treatments have not altered the disease course in IPF patients and because inflammatory cell accumulation is not a prominent feature of the histopathology (12). Instead, defective type II AECs are thought to directly drive fibrogenesis through their failure to reconstitute an intact epithelium and through their altered production of pro-and anti-fibrotic mediators. The development of our model of DT-

mediated injury to type II AEC confirmed the relationship between epithelial injury and lung fibrosis and also afforded us the opportunity to investigate whether inflammation helps translate the epithelial insult into a fibrotic response. In the current study, we identify for the first time, a direct relationship between targeted injury to the type II epithelium, the influx of inflammatory cells, and the deposition of lung collagen. Specifically, DT-mediated injury to type II AECs induced a sustained approximate 2-fold increase in total lung leukocytes. Histologic evaluation in DT-treated DTR+ mice revealed an increased cellularity within the alveolar walls, and this microanatomic location of inflammation coincides with the distribution of collagen deposition reported in the current study (refer to Figures 1B and 4B) and in our initial report of this model (11). This modest degree of inflammation in our model is reminiscent of the relatively sparse inflammation observed in histopathology sections obtained from IPF lungs and contrasts with the exuberant inflammation observed in the lungs of mice treated with bleomycin.

Within the context of this mild inflammatory response, we observed an early and sustained enrichment in the numbers of ExM and their precursors, Ly-6C^{high} monocytes. This finding confirms and extends the results of our recently published study and further substantiates the renewed interest in the hypothesis that macrophages and monocytes contribute to lung scarring (20). To investigate the contribution of the ExM and Ly-6C^{high} monocyte subpopulations to fibrogenesis, we employed double transgenic DTR+ CCR2-deficient mice in which the accrual of these cells within the lung is impaired (24, 25, 38). As expected, CCR2-deficiency completely abrogated the accumulation of ExM and Ly-6C^{high} monocytes in response to alveolar injury but had no effect on AM or Ly-6C^{low} monocytes. The significance of this observation is underscored by our finding that CCR2-deficient mice are substantially protected from fibrosis and mortality in this model. Our observation that DT-treated DTR+:CCR2−/− mice did lose weight (relative to untreated mice and DT-treated WT mice) implies that the protection against fibrosis and mortality was not attributable to an inhibition in lung injury. Collectively, these results suggest that the non-resident ExM and Ly-6C^{high} monocytes are the subsets most likely to contribute to aberrant fibrotic responses in the injured lung. This assertion is supported by a preliminary analysis of IPF patients enrolled in the IPFnet PANTHER trial and the NHLBI-funded COMET trial that revealed the population of CD14+ CD16-monocytes (the human equivalent of murine Ly-6C^{high} monocytes) to be increased in the peripheral blood {B. Moore, University of Michigan; personnel communication and published in abstract form (39)}. These findings additionally complement those of Gibbons and colleagues who reported that monocyte depletion reduced lung fibrosis in mice in response to bleomycin administration or TGF-β overexpression and that fibrosis was exacerbated by the adoptive transfer of Ly-6C^{high} monocytes (15).

The molecular mechanisms by which inflammatory cells contribute to fibrosis are of considerable interest and debate. One increasingly popular hypothesis suggests that lung leukocytes indirectly promote lung fibrogenesis through their effects on local epithelial and mesenchymal cells. Our prior study was the first to demonstrate that ExM were a source of PAI-1 in mice with DT-mediate type II AEC injury. PAI-1 has been implicated in numerous profibrotic processes and we showed that in the absence of PAI-1, mice were protected from lung fibrosis in this model. In addition to PAI-1, in the present study, we show that ExM express mRNA for Arginase-1, and Galectin-3, and an elevated Arginase:iNOS ratio, a pattern consistent with alternative activation. This phenotype, increasingly reported in fibrotic tissues, may serve as a biomarker of scarring (15–17, 19, 31). Furthermore, arginase itself may participate in the fibrotic cascade (40). ExM and their precursors, Ly-6C^{high} monocytes, also express mRNA for the profibrotic cytokines IL-13, and TGF-β which could activate local mesenchymal cells in a paracrine manner.

A second and more controversial hypothesis suggests that lung leukocytes directly contribute to fibrosis by their production and deposition of collagen. Central to the development of this hypothesis has been the identification of fibrocytes as bone marrow derived cells displaying evidence of collagen production within injured tissues (including lung) which develop fibrosis. The results of our studies raise two important questions relevant to this hypothesis. First, are ExM and (or) Ly-6C^{high} monocytes fibrocytes? Second, what is the relative contribution of monocytes and macrophages to collagen deposition? Most broadly defined, fibrocytes are bone-marrow derived cells identified by the expression of CD45 and collagen (as assessed by staining for intracellular collagen and/or the presence of collagen gene expression). Fibrocyte expression of MHC Class II, CD80, CD11b, CCR2, and CXCR4 and their CCR2-dependent accumulation within injured tissues are also reported (23, 36, 37, 41). Based on the above criteria, our data indicate that subsets of both ExM and Ly-6C^{high} monocytes in the lungs of mice with type II AEC injury qualify as fibrocytes. These findings complement those of Niedermeier and colleagues who demonstrated that splenic fibrocytes are derived from CD11b+ GR-1+ (comparable to Ly-6C^{high}) monocytes (42) and that fibrocyte development was influenced by CD4+ T cells and a panel of T cell-associated cytokines (including IL-2, TNFα, IFNγ, and IL-4). Our additional phenotypic characterization provides the first data, to our knowledge, that ExM and Ly-6C^{high} monocytes in the lungs of mice that develop fibrosis express the immunomodulatory costimulatory molecules, PDL-1 and PDL-2. Thus an intriguing direction of future studies will be to determine whether cell-cell interactions between fibrocytes and T cells might influence lung fibrogenesis in this model. Collectively, our results strongly suggest that the term fibrocyte, as broadly defined, consists of a heterogeneous population of cells including subsets of ExM and Ly-6C^{high} monocytes which may promote fibrosis through growth factor, cytokine, and/or collagen production.

With respect to the second question outlined above, the relative contribution of bone marrow-derived cells to lung fibrosis through direct collagen synthesis cannot be answered by our current results. However, our data provide some important insights through the enumeration of CD45+ Col1+ cells and CD45- Col1+ cells in the lungs of 1) DT-treated WT mice, 2) DTR+ mice, and 3) DTR+:CCR2−/− mice (refer to Figure 6A). Using this approach, we observed that the number of CD45+ Col1+ cells in DTR+ mice increased significantly relative to their numbers in WT mice; a similar increase was not observed in the DTR+:CCR2−/− mice which are protected from fibrosis. At the time of peak inflammation (D14), the total number of CD45+:Col1+ cells in the DTR+ mice was approximately half that of CD45- Col1+ population in the same animals. Thus, the CD45+ Col1+ population of cells, although less than the CD45- Col1+ cells, still represented a sizable fraction (≈1/3rd) of the numbers of Col1+ cells. At present, the phenotype of the CD45- Col1+ cells in this model is unknown and we acknowledge that identification of intracellular collagen staining does not reliably account for potential differences in the quantity or rate with which various cell types might deposit matrix constituents in the lungs of these mice. Thus, future studies will be required to more rigorously investigate the relative contribution of the various subsets of cells to collagen production.

In summary, we have established that targeted type II AEC injury induces a modest inflammatory response that is none-the-less significantly enriched for alternatively-activated and profibrotic ExM and Ly-6C^{high} monocytes. The accumulation of these nonresident cells and the development of pulmonary fibrosis in response to targeted alveolar injury is CCR2-dependent. We believe this model system recapitulates many features of pulmonary fibrosis in humans thereby implicating ExM and Ly-6C^{high} monocytes and the CCR2/CCR2-ligand axis as potential therapeutic targets to treat or prevent fibrotic lung disease.

Supplementary Material

Refer to Web version on PubMed Central for supplementary material.

Acknowledgments

We wish to specifically acknowledge and thank our research funding sources including the Quest for Breath Foundation along with the National Institutes of Health and the Department of Veterans Affairs.

The abbreviations used are

AEC	alveolar epithelial cell
AM	alveolar macrophage
CCR2$^{+/+}$ mice	wild type mice expressing CCR2
CCR2$^{-/-}$ mice	syngeneic mice deficient in chemokine receptor 2
DT	diphtheria toxin
DTR	diphtheria toxin receptor
DTR+ mice	mice expressing the diphtheria toxin receptor under the control of the surfactant protein C promoter
ExM	exudate macrophage
IPF	idiopathic pulmonary fibrosis
SPC	surfactant protein C

References

1. Kawanami O, Ferrans VJ, Crystal RG. Structure of alveolar epithelial cells in patients with fibrotic lung disorders. Lab Invest. 1982; 46:39–53. [PubMed: 7054589]
2. Katzenstein AA. Pathogenesis of “fibrosis” in interstitial pneumonia: An electron microscopic study. Human Pathol. 1985; 16:1015–24. [PubMed: 4043950]
3. Kasper M, Haroske G. Alterations in the alveolar epithelium after injury leading to pulmonary fibrosis. Histol Histopathol. 1996; 11:463–83. [PubMed: 8861769]
4. Wang Y, Kuan PJ, Xing C, Cronkhite JT, Torres F, Rosenblatt RL, DiMaio JM, Kinch LN, Grishin NV, Garcia CK. Genetic defects in surfactant protein A2 are associated with pulmonary fibrosis and lung cancer. Am J Hum Genet. 2009; 84:52–9. [PubMed: 19100526]
5. Maitra M, Wang Y, Gerard RD, Mendelson CR, Garcia CK. Surfactant protein A2 mutations associated with pulmonary fibrosis lead to protein instability and endoplasmic reticulum stress. J Biol Chem. 2010; 285:22103–13. [PubMed: 20466729]
6. Thomas AQ, Lane K, Phillips J 3rd, Prince M, Markin C, Speer M, Schwartz DA, Gaddipati R, Marney A, Johnson J, Roberts R, Haines J, Stahlman M, Loyd JE. Heterozygosity for a surfactant protein C gene mutation associated with usual interstitial pneumonitis and cellular nonspecific interstitial pneumonitis in one kindred. Am J Respir Crit Care Med. 2002; 165:1322–8. [PubMed: 11991887]
7. van Moorsel CH, van Oosterhout MF, Barlo NP, de Jong PA, van der Vis JJ, Ruven HJ, van Es HW, van den Bosch JM, Grutters JC. Surfactant protein C mutations are the basis of a significant portion of adult familial pulmonary fibrosis in a dutch cohort. Am J Respir Crit Care Med. 2010; 182:1419–25. [PubMed: 20656946]
8. Young LR, Nogee LM, Barnett B, Panos RJ, Colby TV, Deutsch GH. Usual interstitial pneumonia in an adolescent with ABCA3 mutations. Chest. 2008; 134:192–5. [PubMed: 18628224]
9. Adamson IY, Bowden DH. Origin of ciliated alveolar epithelial cells in bleomycin-induced lung injury. Am J Pathol. 1977; 87:569–80. [PubMed: 68683]

10. Adamson IY, Bowden DH. Bleomycin-induced injury and metaplasia of alveolar type 2 cells. Relationship of cellular responses to drug presence in the lung. Am J Pathol. 1979; 96:531–44. [PubMed: 89815]

11. Sisson TH, Mendez M, Choi K, Subbotina N, Courey A, Cunningham A, Dave A, Engelhardt JF, Liu X, White ES, Thannickal VJ, Moore BB, Christensen PJ, Simon RH. Targeted injury of type II alveolar epithelial cells induces pulmonary fibrosis. Am J Respir Crit Care Med. 2010; 181:254–63. [PubMed: 19850947]

12. Selman M, King TE, Pardo A. Idiopathic pulmonary fibrosis: prevailing and evolving hypotheses about its pathogenesis and implications for therapy. Ann Intern Med. 2001; 134:136–51. [PubMed: 11177318]

13. Okuma T, Terasaki Y, Kaikita K, Kobayashi H, Kuziel WA, Kawasuji M, Takeya M. C-C chemokine receptor 2 (CCR2) deficiency improves bleomycin-induced pulmonary fibrosis by attenuation of both macrophage infiltration and production of macrophage-derived matrix metalloproteinases. J Pathol. 2004; 204:594–604. [PubMed: 15538737]

14. Baran CP, Opalek JM, McMaken S, Newland CA, O'Brien JM Jr, Hunter MG, Bringardner BD, Monick MM, Brigstock DR, Stromberg PC, Hunninghake GW, Marsh CB. Important roles for macrophage colony-stimulating factor, CC chemokine ligand 2, and mononuclear phagocytes in the pathogenesis of pulmonary fibrosis. Am J Respir Crit Care Med. 2007; 176:78–89. [PubMed: 17431224]

15. Gibbons MA, MacKinnon AC, Ramachandran P, Dhaliwal K, Duffin R, Phythian-Adams AT, van Rooijen N, Haslett C, Howie SE, Simpson AJ, Hirani N, Gauldie J, Iredale JP, Sethi T, Forbes SJ. Ly6Chi monocytes direct alternatively activated profibrotic macrophage regulation of lung fibrosis. Am J Respir Crit Care Med. 2011; 184:569–81. [PubMed: 21680953]

16. Mora AL, Torres-Gonzalez E, Rojas M, Corredor C, Ritzenthaler J, Xu J, Roman J, Brigham K, Stecenko A. Activation of alveolar macrophages via the alternative pathway in herpesvirus-induced lung fibrosis. Am J Respir Cell Mol Biol. 2006; 35:466–73. [PubMed: 16709958]

17. Gangadharan B, Hoeve MA, Allen JE, Ebrahimi B, Rhind SM, Dutia BM, Nash AA. Murine gammaherpesvirus-induced fibrosis is associated with the development of alternatively activated macrophages. J Leukoc Biol. 2008; 84:50–8. [PubMed: 18436582]

18. Murray LA, Chen Q, Kramer MS, Hesson DP, Argentieri RL, Peng X, Gulati M, Homer RJ, Russell T, van Rooijen N, Elias JA, Hogaboam CM, Herzog EL. TGF-beta driven lung fibrosis is macrophage dependent and blocked by Serum amyloid P. Int J Biochem Cell Biol. 2011; 43:154–62. [PubMed: 21044893]

19. Sun L, Louie MC, Vannella KM, Wilke CA, LeVine AM, Moore BB, Shanley TP. New concepts of IL-10-induced lung fibrosis: fibrocyte recruitment and M2 activation in a CCL2/CCR2 axis. Am J Physiol Lung Cell Mol Physiol. 2011; 300:L341–53. [PubMed: 21131395]

20. Osterholzer JJ, Christensen PJ, Lama V, Horowitz JC, Hattori N, Subbotina N, Cunningham A, Lin Y, Murdock BJ, Morey RE, Olszewski MA, Lawrence DA, Simon RH, Sisson TH. PAI-1 Promotes the Accumulation of Exudate Macrophages and Worsens Pulmonary Fibrosis Following Type II Alveolar Epithelial Cell Injury. J Pathol. 2012; 228(2):170–80. [PubMed: 22262246]

21. Osterholzer JJ, Curtis JL, Polak T, Ames T, Chen GH, McDonald R, Huffnagle GB, Toews GB. CCR2 mediates conventional dendritic cell recruitment and the formation of bronchovascular mononuclear cell infiltrates in the lungs of mice infected with Cryptococcus neoformans. J Immunol. 2008; 181:610–20. [PubMed: 18566428]

22. Tusher VG, Tibshirani R, Chu G. Significance analysis of microarrays applied to the ionizing radiation response. Proc Natl Acad Sci U S A. 2001; 98:5116–21. [PubMed: 11309499]

23. Moore BB, Murray L, Das A, Wilke CA, Herrygers AB, Toews GB. The role of CCL12 in the recruitment of fibrocytes and lung fibrosis. Am J Respir Cell Mol Biol. 2006; 35:175–81. [PubMed: 16543609]

24. Osterholzer JJ, Chen GH, Olszewski MA, Zhang YM, Curtis JL, Huffnagle GB, Toews GB. Chemokine receptor 2-mediated accumulation of fungicidal exudate macrophages in mice that clear cryptococcal lung infection. Am J Pathol. 2011; 178:198–211. [PubMed: 21224057]

25. Osterholzer JJ, Chen GH, Olszewski MA, Curtis JL, Huffnagle GB, Toews GB. Accumulation of CD11b+ lung dendritic cells in response to fungal infection results from the CCR2-mediated

recruitment and differentiation of Ly-6Chigh monocytes. J Immunol. 2009; 183:8044–53. [PubMed: 19933856]

26. Hattori N, Degen JL, Sisson TH, Liu H, Moore BB, Pandrangi RG, Simon RH, Drew AF. Bleomycin-induced pulmonary fibrosis in fibrinogen-null mice. J Clin Invest. 2000; 106:1341–50. [PubMed: 11104787]
27. Tighe RM, Liang J, Liu N, Jung Y, Jiang D, Gunn MD, Noble PW. Recruited Exudative Macrophages Selectively Produce CXCL10 after Noninfectious Lung Injury. Am J Respir Cell Mol Biol. 2011; 45:781–8. [PubMed: 21330464]
28. Lin KL, Suzuki Y, Nakano H, Ramsburg E, Gunn MD. CCR2+ monocyte-derived dendritic cells and exudate macrophages produce influenza-induced pulmonary immune pathology and mortality. J Immunol. 2008; 180:2562–72. [PubMed: 18250467]
29. Winter C, Herbold W, Maus R, Langer F, Briles DE, Paton JC, Welte T, Maus UA. Important role for CC chemokine ligand 2-dependent lung mononuclear phagocyte recruitment to inhibit sepsis in mice infected with Streptococcus pneumoniae. J Immunol. 2009; 182:4931–7. [PubMed: 19342672]
30. Skold M, Behar SM. Tuberculosis triggers a tissue-dependent program of differentiation and acquisition of effector functions by circulating monocytes. J Immunol. 2008; 181:6349–60. [PubMed: 18941226]
31. Hardie WD, Glasser SW, Hagood JS. Emerging concepts in the pathogenesis of lung fibrosis. Am J Pathol. 2009; 175:3–16. [PubMed: 19497999]
32. Phillips RJ, Burdick MD, Hong K, Lutz MA, Murray LA, Xue YY, Belperio JA, Keane MP, Strieter RM. Circulating fibrocytes traffic to the lungs in response to CXCL12 and mediate fibrosis. J Clin Invest. 2004; 114:438–46. [PubMed: 15286810]
33. Vannella KM, McMillan TR, Charbeneau RP, Wilke CA, Thomas PE, Toews GB, Peters-Golden M, Moore BB. Cysteinyl leukotrienes are autocrine and paracrine regulators of fibrocyte function. J Immunol. 2007; 179:7883–90. [PubMed: 18025235]
34. McMillan TR, Moore BB, Weinberg JB, Vannella KM, Fields WB, Christensen PJ, van Dyk LF, Toews GB. Exacerbation of established pulmonary fibrosis in a murine model by gammaherpesvirus. Am J Respir Crit Care Med. 2008; 177:771–80. [PubMed: 18187693]
35. Pilling D, Fan T, Huang D, Kaul B, Gomer RH. Identification of markers that distinguish monocyte-derived fibrocytes from monocytes, macrophages, and fibroblasts. PLoS One. 2009; 4:e7475. [PubMed: 19834619]
36. Mehrad B, Burdick MD, Strieter RM. Fibrocyte CXCR4 regulation as a therapeutic target in pulmonary fibrosis. Int J Biochem Cell Biol. 2009; 41:1708–18. [PubMed: 19433312]
37. Moore BB, Kolodsick JE, Thannickal VJ, Cooke K, Moore TA, Hogaboam C, Wilke CA, Toews GB. CCR2-mediated recruitment of fibrocytes to the alveolar space after fibrotic injury. Am J Pathol. 2005; 166:675–84. [PubMed: 15743780]
38. Serbina NV, Pamer EG. Monocyte emigration from bone marrow during bacterial infection requires signals mediated by chemokine receptor CCR2. Nat Immunol. 2006; 7:311–7. [PubMed: 16462739]
39. Moore BF, CD, Wilke CA, Toews GB. Circulating Monocytes In Idiopathic Pulmonary Fibrosis (ipf) Patients Express Tlr9 And Cd206. Am J Respir Crit Care Med. 2011; 183:A4277.
40. Wehling-Henricks M, Jordan MC, Gotoh T, Grody WW, Roos KP, Tidball JG. Arginine metabolism by macrophages promotes cardiac and muscle fibrosis in mdx muscular dystrophy. PLoS One. 2010; 5:e10763. [PubMed: 20505827]
41. Strieter RM, Keeley EC, Hughes MA, Burdick MD, Mehrad B. The role of circulating mesenchymal progenitor cells (fibrocytes) in the pathogenesis of pulmonary fibrosis. J Leukoc Biol. 2009; 86:1111–8. [PubMed: 19581373]
42. Niedermeier M, Reich B, Rodriguez Gomez M, Denzel A, Schmidbauer K, Gobel N, Talke Y, Schweda F, Mack M. CD4+ T cells control the differentiation of Gr1+ monocytes into fibrocytes. Proc Natl Acad Sci U S A. 2009; 106:17892–7. [PubMed: 19815530]

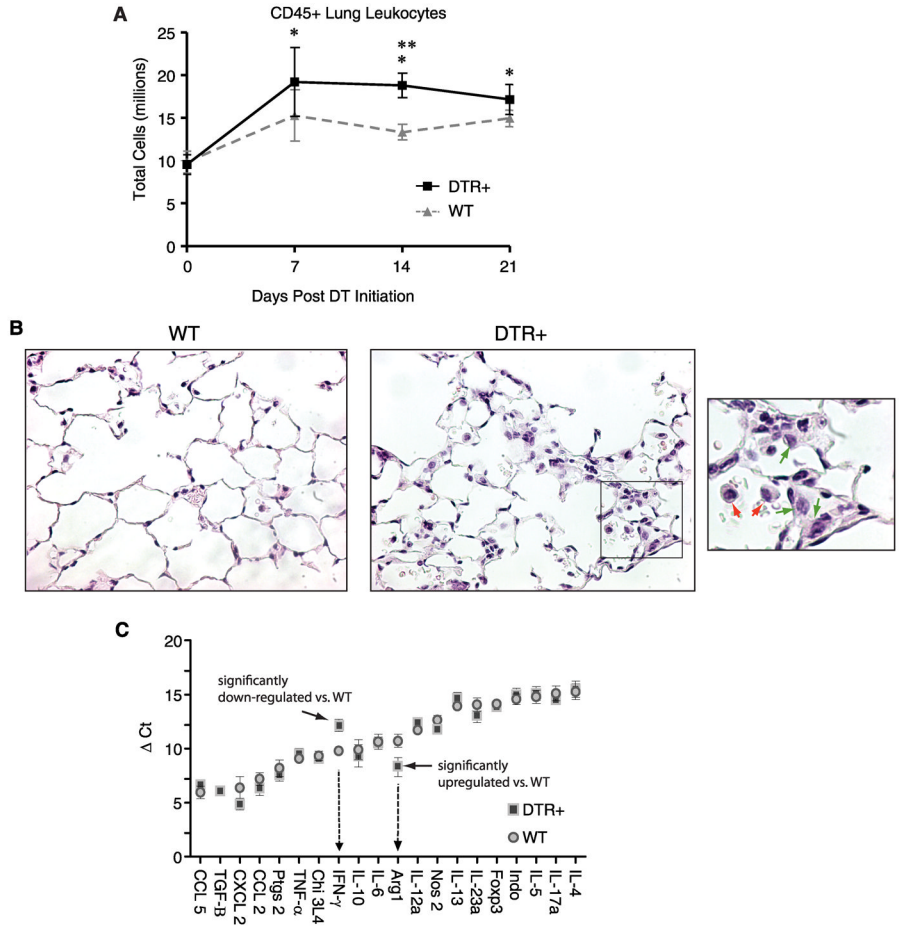

Figure 1. Targeted injury to type II AEC promotes lung inflammation

Diphtheria toxin was administered daily for 14 days to either WT (DTR−) or DTR+ mice. (**A**) Lung cells from individual mice were isolated from untreated mice (D0) and at 7, 14, and 21 days after the onset of DT treatment. Cells were antibody-stained and flow cytometric analysis was used to identify and enumerate total numbers of CD45+ lung leukocytes. Data are mean ± SEM of 8–12 DT-treated mice per time point (from three separate experiments) assayed individually; DTR+ mice, black squares and solid lines; WT mice, gray triangles and dashed lines; * $p<0.05$ vs. Day 0 (uninfected) of mice of the same DTR expression profile; ** $p<0.05$ when values from WT mice or DTR+ mice were compared against each other at the designated time point. (**B**) Representative photomicrographs of lung sections (H & E staining; 40x objective) obtained from DT-treated WT (left panel) and DTR+ mice (right panel and inset). Note the presence of increased cellularity in the alveolar regions of DTR+ mice with evidence of large cells both with alveolar airspaces (inset; orange arrows) and within thickened interstitial infiltrates (inset; green arrows). (**C**) A limited gene array was performed on RNA extracted from enriched lung leukocyte populations of WT mice (circles) or DTR+ mice (squares) following 14 days of DT-treatment. Data is plotted as the cycle time difference (ΔCt) between the target gene and the β-actin gene. Solid arrows indicate significant differences in gene expression between WT and DTR+ mice.

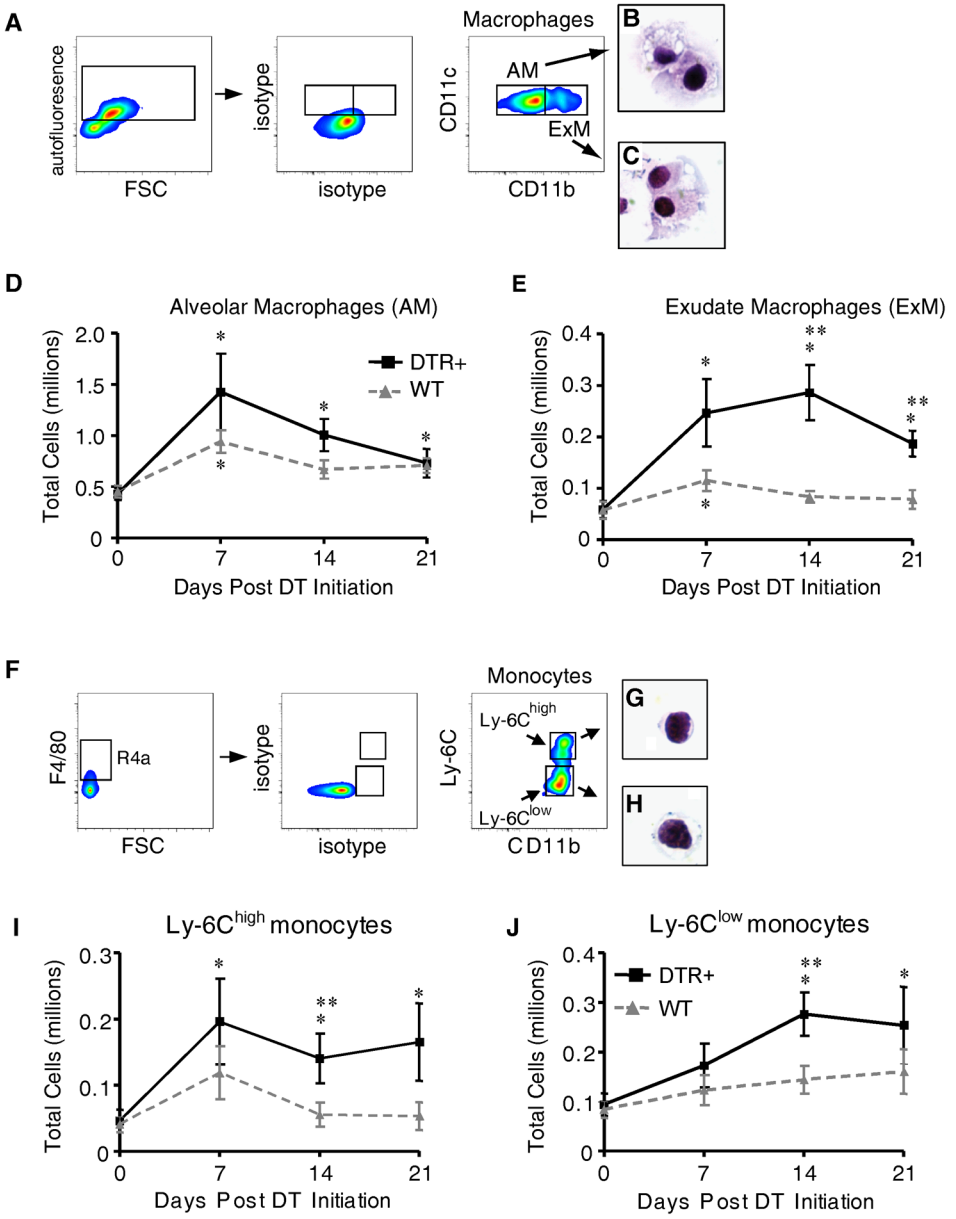

Figure 2. Exudate macrophages and Ly-6C^{high} monocytes accumulate in mice with targeted injury to type II AEC

Diphtheria toxin was administered per protocol for 14 days to either WT (DTR−) or DTR+ mice. (**A–J**) Lung cells isolated from untreated mice (D0) and at 7, 14, and 21 days after the onset of DT treatment were stained with specific antibodies and analyzed by flow cytometric analysis as described in Materials and Methods and Supplemental Figure S1. (A) Gating strategy used to identify AM and ExM among lung leukocytes obtained from DTR+ mice after 14 days of DT-treatment. Initial gating (not shown) on CD45$^+$ lung leukocytes excludes debris, lymphocytes, and CD11c-negative cells (refer to Figure S1). Within the CD11c-postive populations, a plot of FL-3 vs. FSC (left dot plots) distinguishes larger autofluorescent macrophages (AF$^+$) from smaller non-autofluorescent cells. Amongst AF$^+$ macrophages, plots of isotype controls (middle dot plots) and CD11c vs. CD11b (right dot plots) distinguish AM (as AF$^+$ CD11c$^+$ CD11b$^-$, gate AM) and ExM (as AF$^+$ CD11c$^+$

CD11b^{+}, gate ExM). (**B, C**) Representative photomicrographs of AM (**B**) and ExM (**C**) obtained by flow sorting of lung leukocytes at D14 (100x objective; H&E stain). (**D, E**) Total numbers of AM (**D**) and ExM (**E**) present in the lungs of WT or DTR+ mice at each timepoint. (**F**) Gating strategy used to identify Ly-6C^{low} and Ly-6C^{high} monocytes among lung leukocytes obtained from DTR+ mice after 14 days of DT-treatment. Initial gating (not shown) on CD45^{+} lung leukocytes excludes debris, lymphocytes, granulocytes, and CD11c-positive cells (refer to Figure S1). Within the SSC^{low} CD11c-negative population (left dot pot), a gate of F4/80 vs FSC identifies F4/80-positive monocytes. Next, plots of isotype controls (middle dot plot) and Ly-6C vs. CD11b (right dot plot) identify Ly-6C^{high} monocytes (gate Ly-6C^{high}) and Ly-6C^{low} monocytes (gate Ly-6C^{low}). (**G, H**) Representative photomicrographs of Ly-6C^{high} monocytes (**G**) and Ly-6C^{low} monocytes (**H**) obtained by flow sorting of lung leukocytes at D14 (100x objective; H&E stain). (**I, J**) Total numbers of Ly-6C^{high} monocytes (**I**) and Ly-6C^{low} monocytes (**J**) present in the lungs of WT or DTR+ mice at each timepoint. Total macrophage and monocyte numbers were calculated by multiplying the frequency of each population (using the gating strategy described above) by the total number of CD45^{+} lung leukocytes at each time point. Data represent mean ± SEM of 8–12 mice assayed individually per time point. * $p<0.05$ ANOVA vs. Day 0 (untreated) of mice of the same DTR expression profile; ** $p<0.05$ when values from WT mice or DTR+ mice were compared against each other at the designated time point.

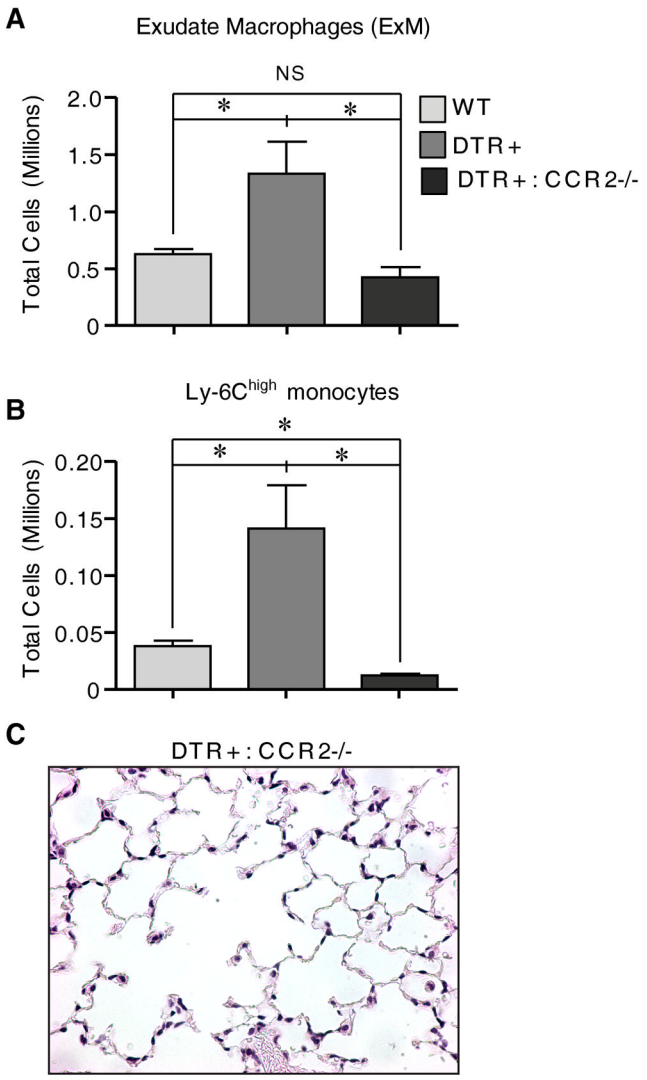

Figure 3. Accumulation of exudate macrophages and Ly-6C^{high} monocytes in mice with targeted type II AEC injury is CCR2-dependent

Diphtheria toxin was administered for 14 days per protocol to: 1) WT mice (DTR−:CCR2+/+), 2) DTR+ mice (DTR+:CCR2+/+), and 3) DTR+:CCR2−/− mice. Lung leukocytes from individual mice were isolated and antibody stained. Multi-parameter flow cytometric analysis was used to identify and enumerate total numbers of (**A**) ExM and (**B**) Ly-6C^{high} monocytes. Data are mean ± SEM of 4–5 DT-treated mice per strain assayed individually. * P values <0.05 between groups at the same time point were considered significant. (**C**) Photomicrograph of a representative lung section (H & E staining; 40x objective) from a DT-treated DTR+ mouse deficient in CCR2. Note the relative absence of inflammation.

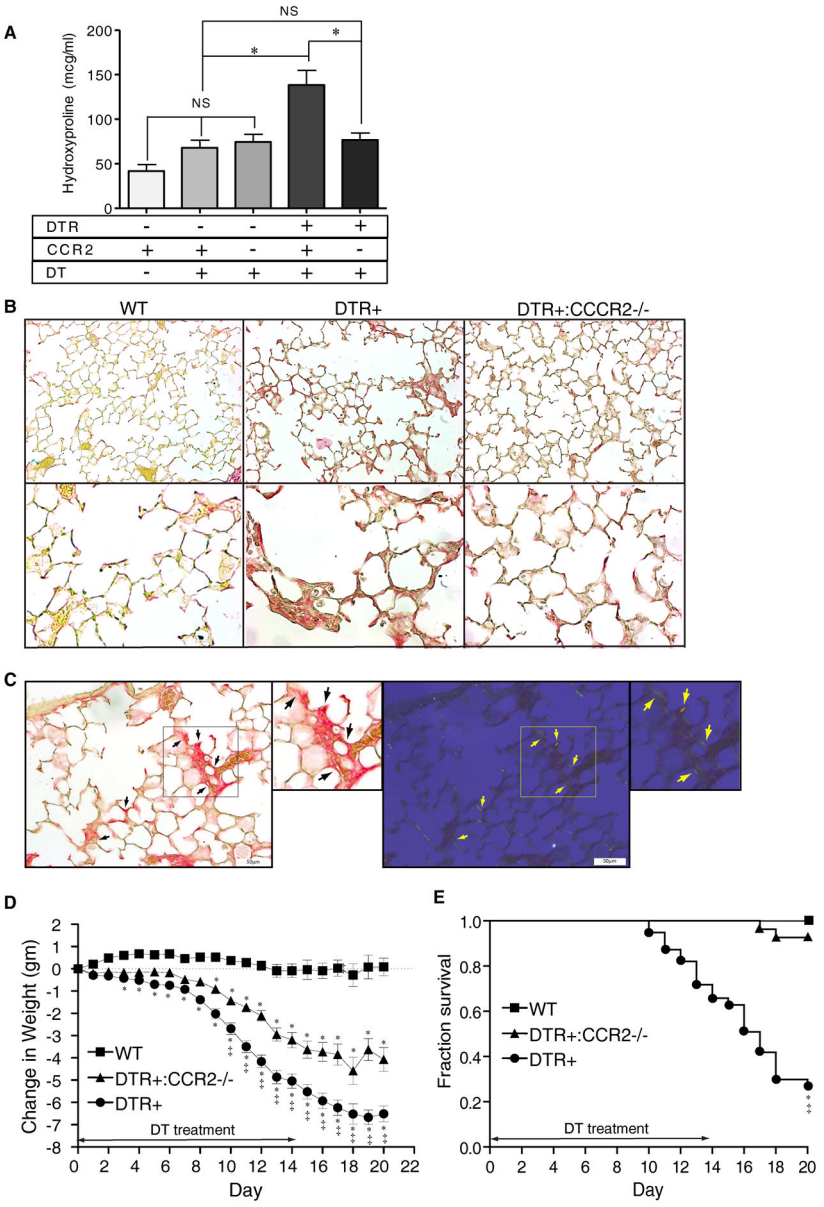

Figure 4. CCR2 expression mediates lung collagen deposition, weight loss, and increases mortality following injury to type II AEC

(A) Diphtheria toxin was administered for 14 days per protocol to: 1) WT mice (DTR −:CCR2+/+), 2) CCR2-deficient mice (DTR−:CCR2−/−), 3) DTR+ mice (DTR+:CCR2+/+), and 4) DTR+:CCR2−/−mice. An additional group of control WT mice received daily intraperitoneal injections of PBS for 14 days. Lungs were harvested on day 21 and analyzed for hydroxyproline content. Results are reported as the mean concentration in μg/ml ± SEM (n = 6 to 8). P values <0.05 between groups were considered significant. (B) Photomicrographs taken of lung sections obtained from DT-treated WT mice (left panels), DTR+ mice (middle panels), and DTR+:CCR2−/− mice (right panels) at Day 21 (one week after completing DT treatment) and stained with picrosirius red to identify collagen (top panels, 20x objective, bottom panels 40x objective). Note the increase in subepithelial collagen staining (red color) observed in lungs from DTR+ mice which is not observed in WT mice and minimal in DTR:CCR2−/− mice. (C) Photomicrographs (20x objective) of

picrosirius-stained lung sections obtained from DT-treated DTR+ mice (D21) viewed by bright field (left panel and inset) and cross-polarized (right panel and inset) microscopy. Black arrows (left panels) identify regions of increased picrosirius staining. Yellow arrows (right panels) identify corresponding regions displaying birefringence (yellow fluorescence) indicative of co-aligned collagen. (D, E) Weight loss (D) and survival (E) in WT, DTR+, and DTR+:CCR2−/− mice treated with DT per protocol for 14 days. * $p<0.05$ vs DT-treated WT mice; ‡ $p<0.05$ vs DT-treated DTR+:CCR2−/− mice.

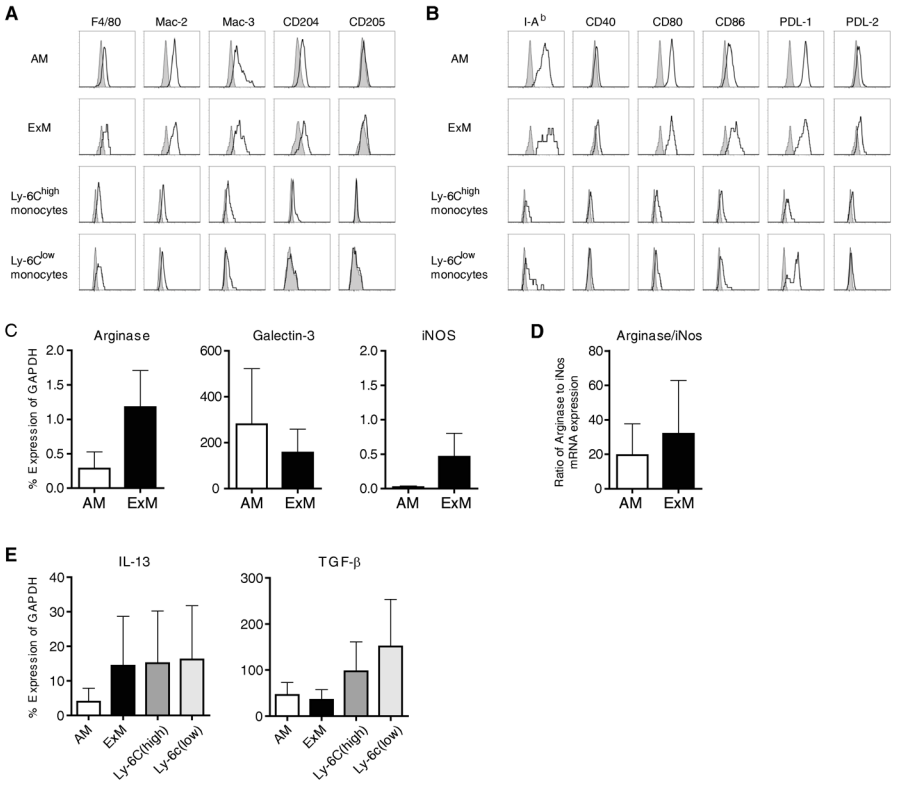

Figure 5. Immunophenotype of ExM and Ly-6C^{high} monocytes in mice with type II AEC injury

(**A, B**) Representative histograms (four-decade log scale) of ExM and Ly-6C^{high} monocytes pooled from four individual DTR+ mice at D14 of DT-treatment displaying their expression of (**A**) macrophage-associated proteins (F4/80, Mac-2, Mac-3, CD204, CD205) and (**B**) MHC Class II (I–A^{d}) and costimulatory molecules (CD40, CD80, CD86, PDL-1, and PDL-2). Shaded histogram, isotype staining; open histogram, specific staining. The experiment was repeated once with similar results. (**C–E**) Designated subsets of lung macrophages and monocytes were purified (≈95% by cell sorting) from pooled populations of lung leukocytes obtained from DTR+ mice (n=5 mice) at D14 of DT-treatment. mRNA obtained from each subset was assessed by qRT-PCR. Specific gene expression is expressed as a percentage of GAPDH (Methods). Values represent the average ± SEM from three independently-performed experiments. (C, D) AM and ExM expression of genes associated with (**C**) alternative (Arginase-1, Galectin-3) or classical (iNOS) macrophage activation. (**D**) Ratio of Arginase:iNOS gene expression (as calculated for each experiment). (**E**) Macrophage and monocyte expression of profibrotic cytokine genes, IL-13 and TGF-β.

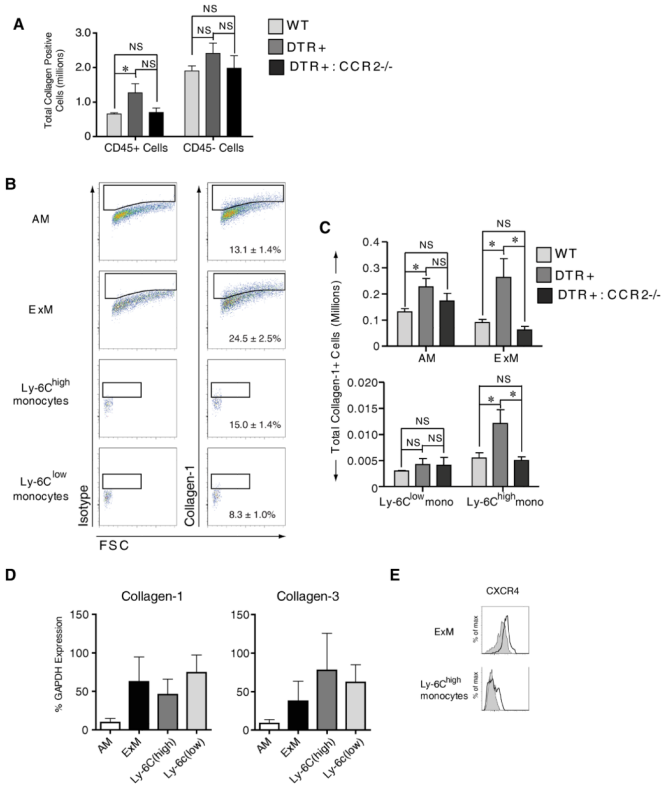

Figure 6. CCR2 mediates the specific accumulation of type I collagen positive exudate macrophages and Ly-6C^{high} monocytes in mice with targeted type II AEC injury

(**A**–C) Flow cytometric analysis was performed on cells obtained from the lungs of DT-treated: 1) WT mice, 2) DTR+ mice, and 3) DTR+:CCR2−/− mice (n=4–5 mice per group at D14 of DT treatment) for the detection of intracellular Collagen-1 relative to isotype control staining. (A) Total numbers of Collagen-1 positive CD45+ cells (lung leukocytes) and CD45- cells (non-leukocytes). Data are mean ± SEM of 4–5 DT-treated mice per strain assayed individually; * P values <0.05. (B) Representative histograms depicting isotype control staining (left column) and Collagen-1 staining (right column) on each subset of lung macrophages and monocytes. Percentages indicate average Collagen-positive staining for each subset ± SEM. (C) Total numbers of Collagen-1 positive macrophages and monocytes. (D) Defined macrophage and monocyte subsets were purified (≈95% by cell sorting) from pooled populations of lung leukocytes obtained from DT-treated DTR+ mice (n=5 mice) at D14 of DT-treatment. mRNA obtained from each subset was obtained and assessed by qRT-PCR for expression of Collagen-1 and Collagen 3. Specific gene expression was expressed as a percentage of GAPDH (Methods). Values represent the average ± SEM from three separate experiments. (E) Representative histograms depicting the expression of CXCR4 on ExM (top histograms) and Ly-6C^{high} monocytes (bottom histograms) as assessed by flow cytometric analysis performed on lung leukocytes obtained from DT-treated DTR+ mice (n=5) at D14 of DT-treatment. Shaded histogram, isotype staining; open histogram, CXCR4 staining.